Nanosecond Intra-Ionic Chloride Photo-Oxidation

Alexander M. Deetz, Matthew J. Goodwin, Erin A. Kober, and Gerald J. Meyer*

Department of Chemistry, University of North Carolina at Chapel Hill,
Chapel Hill, NC 27599
gjmeyer@email.unc.edu

ABSTRACT

Transition metal photocatalysts capable of oxidizing chloride are rare, yet serve as an attractive means to controllably generate chlorine atoms, which have continued to garner the interest of researchers for notable applications in photoredox catalysis and solar energy storage. Herein, a new series of four Ir-photocatalysts with different dicationic chloride-sequestering ligands were synthesized and characterized to probe the relationship between chloride binding affinity, ion pair solution structures, and rate constants for chloride photo-oxidation in acetonitrile at room temperature. The substituents on the quaternary amines of dicationic bipyridine ligands had negligible effect on the photocatalyst excited-state reduction potential, yet dramatically influenced the affinity for chloride binding, indicating that synthetic design can be utilized to independently tune these important properties. An inverse correlation was observed between the equilibrium constant for chloride ion pairing and the rate constant for intra-ionic chloride oxidation. Exceptions to this trend suggest structural differences in the ion-paired solution structures, which were probed by ^{1}H NMR binding experiments. This study provides new insights into light-induced oxidation of ion-paired substrates, a burgeoning approach that offers to circumvent diffusional constraints of photocatalysts with short excited-state lifetimes. Ground-state association of chloride with these photocatalysts enables intra-ionic chloride oxidation on a rapid, nanosecond timescale.

INTRODUCTION

Halides and halogen atoms are of central importance to emerging applications in photocatalysis, solar energy conversion, environmental chemistry, and membrane chemistry.[1,2] Examples include photoredox catalysis where chlorine atoms have been utilized to activate C–H bonds and drive new synthetic transformations to yield value added organic compounds.[3–12,13–19] Halides are intimately involved in solar light harvesting and carrier transport in high efficiency perovskite-type solar cells.[20,21] Additionally, halides undergo redox and Lewis acid–base chemistry in dye-sensitized[22–24] and hydrohalic acid (HX, where X = I, Br, Cl) splitting solar cells.[25–29] Thus, optimization of halogen and halide chemistry and their redox behavior are especially relevant to solar energy storage and organic synthesis.

From the expansive literature of applications utilizing halide redox chemistry, a significant subset would benefit from a photocatalyst (PC) assembly that recognizes, binds, and oxidizes halides ions by intra-ionic electron transfer. For instance, a PC that favorably binds halides in a dye-sensitized solar cell offers the advantage of maintaining a high concentration of halide ions at the surface–solution interface. Additionally, association of halides with photocatalysts in the ground state can be utilized as a technique to circumvent the limitations of short-lived excited states for diffusional reactivity in C–H functionalization chemistry.[19] Moreover, selective recognition of chloride from a ubiquitous source such as seawater where subsequent chloride oxidation can enable fuel-forming reactions is a highly sought-after goal in the context of solar energy storage.[25,30] Toward these aims, a number of approaches have been described to promote association of halides with photocatalysts and the influence on excited-state reactivity has been well documented, particularly with ruthenium polypyridyl PCs.[1,31]

Association of iodide with the ruthenium photocatalyst $[Ru(deeb)_2(tmam)]^{4+}$, where deeb = 4,4’-diethylester-2,2’-bipyridine and tmam = 4,4′- bis[(trimethylamino)methyl]-2,2′-bipyridine, resulted in excited-state electron transfer from the ion-paired iodide to the metal center.[32] In this work, quenching of $[Ru(deeb)_2(tmam)]^{4+}$ by the ion-paired iodide resulted in behavior consistent with the textbook definition[33] of static quenching where ground-state adduct formation rendered the photocatalyst “nonluminescent”. In another study, $[Ru(dtb)_2(dea)]^{2+}$, where dtb = 4,4’-di-*tert*-butyl-2,2’-bipyridine and dea = 4,4’-diethanolamide-2,2’-bipyridine, was determined to strongly ion pair iodide, yet was only quenched through a dynamic (*i.e.*, diffusional) quenching mechanism by iodide ions that were freely diffusing in solution.[34] It was rationalized that the ion-paired iodide

was stabilized to such a large extent by favorable interactions with the dea ligand that the photocatalyst was no longer able to oxidize the sequestered ion. These examples represent two extremes of the influence of ground-state association on excited state quenching that encompass the majority of behaviors described in the scientific literature.

On the one hand, interactions that promote selective sequestration of halide ions can provide such significant stabilization that desirable "intra-ionic" excited-state reactivity is inaccessible. At the other extreme, the classic textbook definition states that static quenching by a pre-associated quencher renders the photocatalyst completely nonluminescent.[33] Despite this commonly accepted textbook definition, this need not be the case. In fact, luminescent excited states of photocatalysts ion paired with iodide or bromide ions were recently reported and their electron transfer kinetics were quantified by picosecond luminescence spectroscopy.[35] In this work, we show that this behavior can be generalized to the much more challenging oxidation of chloride ions. We emphasize that examples of excited-state oxidation of chloride are rare, yet offer greater potential for energy storage[25,36] and synthetic chemistry applications[5] than the more commonly studied halide congeners. Moreover, herein we report a new series of iridium photocatalysts that bear pendant cationic ammonium groups toward the goal of untangling the delicate interplay of halide binding and excited-state reactivity. These PCs exhibit remarkably similar photophysical characteristics and excited-state reduction potentials, but with pronounced differences in their halide-binding affinities. The relationship between association constants, ion-pair structure, and intra-ionic electron transfer are discussed.

EXPERIMENTAL

Materials.

Argon gas (Airgas, 99.998%) was passed through a Drierite drying tube before use. Acetonitrile (Burdick and Jackson, 99.98%), d_3-acetonitrile (Cambridge Isotope, 99.8%), chloroform (Fisher, 99.98%), and methanol (Aldrich, 99.5%) were used as received. Tetrabutylammonium chloride (TBACl, Sigma-Aldrich, ≥ 99.0%) was recrystallized from acetone and diethyl ether and stored in a desiccator with Drierite. Tetrabutylammonium hexafluorophosphate ($TBAPF_6$, Sigma-Aldrich, for electrochemical analysis, ≥ 98%), [2,2'-bipyridine]-4,4'-diyldimethanol (Ambeed, 97%), *N,N*-dimethylaniline (Sigma-Aldrich, 99%), quinuclidine (Sigma-Aldrich, 97%), and triethylamine (Sigma-Aldrich, ≥ 99.5%) were used as

received. The [Ir(dF-(CF_3)-ppy)$_2$(4,4'-(CF_3)$_2$-2,2'-bpy)][PF_6], [Ir(dF-(CF_3)-ppy)$_2$(5,5'-(CF_3)$_2$-2,2'-bpy)][PF_6], [Ir(dF-(CF_3)-ppy)$_2$(bpy)][PF_6], and [Ir(dF-(CF_3)-ppy)$_2$(dtb)][PF_6], where dtb is 4,4'-(tert-butyl)$_2$-2,2'-bipyridine were purchased from Strem. The tmam ligand[32,37] and Ir-tmam photocatalyst[35] were prepared following previously reported procedures.

NMR Characterization and Titrations.

All NMR spectra were obtained at room temperature using Varian INOVA Neo 600 MHz, Bruker Avance III 500 MHz, and Bruker Avance Neo 400 MHz spectrometers. ^{13}C NMR spectra were decoupled to {^{1}H}. ^{1}H and ^{13}C chemical shifts were referenced to the residual solvent peak (for acetonitrile, ^{1}H δ = 1.94 ppm for C***H***D_2CN and ^{13}C δ = 1.32 ppm for ***C***D_3CN).[38] The following abbreviations are used in reporting NMR data: s = singlet, d = doublet, t = triplet, q = quartet, hept = heptet, m = multiplet, app = apparent, br = broad. For chloride titration experiments, a known quantity of Ir photocatalyst (typically ~4 mg, 0.275 μmol) was dissolved in 3.0 mL of CD_3CN ([Ir] ≈ 0.9 mM) and 0.60 mL of this solution was placed into a standard 5 mm NMR tube. The chloride-containing titrating solution was prepared by dissolving a known quantity of TBACl (~10 mg) in 2.0 mL of the remaining Ir photocatalyst stock solution such that the photocatalyst concentration was constant throughout the titration. The chloride-containing solution was added incrementally by a Hamilton gastight syringe to the NMR tube, which was inverted 10 times after each addition. The spectrometer was re-shimmed after each addition of chloride solution to ensure homogeneity of the magnetic field. For Ir-team, Ir-tmam, and Ir-quin, the chemical shifts for each hydrogen resonance were tabulated as a function of chloride concentration and the changes were fit to a 1:2 binding model (photocatalyst/chloride) using the Supramolecular.org software applying the Nelder–Mead method to determine the first and second equilibrium constants for halide binding.[39–41] For Ir-pham, the hydrogen resonances labeled "k", "f", "l", "m", and "e" in Figure S19 were omitted from the fit due to their overlapping chemical shifts and an averaged value was used for the hydrogens labeled "j".

UV–Vis Absorption.

UV–Vis absorption spectra were recorded on a Varian Cary 60 UV–Vis spectrophotometer with a scan rate of 2000 nm/min.

Photoluminescence Measurements.

Fresh solutions of Ir photocatalyst were prepared for each experiment with [Ir] = ~30 μM in acetonitrile such that the absorbance of photocatalyst was ~0.065 at the 420 nm excitation wavelength. The exact concentrations of [Ir] were back calculated using the molar extinction coefficients reported herein. A 3.0 mL aliquot of the photocatalyst solution was added to a custom-made quartz cuvette and sealed with a septum. A known quantity of TBACl (~2 mg) was dissolved in 2.0 mL of the remaining photocatalyst solution such that [Ir] was constant throughout the titration and sealed with a septum. Both solutions were deaerated by sparging with argon for at least 30 min. The sparging argon was "pre-wet" by bubbling through neat acetonitrile to minimize solvent evaporation and concentration changes. The halide-containing solution was then titrated into the sealed cuvette through the septum by a gastight Hamilton syringe in increments of ≥ 10 μL additions.

Steady-state PL spectra were recorded on a Horiba Fluorolog 3 fluorimeter and corrected by calibration with a standard tungsten-halogen lamp. Samples were excited at 420 nm and PL was monitored from 430 to 830 nm. The intensity was integrated for 0.1 s at 1 nm resolution and averaged over 3 scans.

Pulsed-light excitation was achieved with a Photon Technology International (PLI) GL-301 dye laser with an excitation centered at 445 nm that was pumped by a PTI GL-3300 nitrogen laser with a pulse width of ~2 ns. The PL was detected by a Hamamatsu R928 PMT optically coupled to a ScienceTech Model 9010 monochromator terminated into a LeCroy Waverunner LT322 oscilloscope. Decays were monitored at 540 nm (unless otherwise indicated) and averaged over 180 pulses. The decays were fit to either a monoexponential or biexponential function using a Levenberg–Marquardt iteration algorithm from which the excited-state lifetime was extracted as a function of chloride concentration. When biexponential kinetics were applicable, the chloride-concentration-independent lifetime (*i.e.*, intra-ionic or static process) was fit as a shared parameter across all non-zero chloride concentrations.

Stern–Volmer Analysis.

The decrease in excited-state lifetimes for the diffusional quenching component were first order in halide concentration, $[X^-]$, and were plotted and fit following the Stern–Volmer relationship:

$$\frac{\tau_0}{\tau} = 1 + K_{SV}[X^-] = 1 + k_q\tau_0[X^-]$$

The plots for τ_0/τ were fit to a line using a Levenberg–Marquardt iteration algorithm. In all cases, the fits had a y-intercept near the anticipated value of 1 but were not constrained in the reported data. The dynamic quenching rate constant, k_q, was extracted from the slope of the best fit line (K_{SV}) using the initial photocatalyst lifetime (without chloride quencher present) measured at the beginning of the titration experiment.

Electrochemistry.

Cyclic voltammetry (CV) experiments were performed with a CH Instruments (CHI660D) Potentiostat in a one-compartment cell, using a platinum working electrode, platinum counter electrode, and a non-aqueous Ag/Ag^+ pseudo-reference electrode that was externally referenced to ferrocene ($Fe(Cp)_2$, +630 mV vs NHE). The cyclic voltammograms were recorded with a scan rate of 100 mV s^{-1}. Experiments were performed in acetonitrile with 0.1 M $TBAPF_6$ supporting electrolyte.

Data Analysis.

NMR spectra were processed using MestReNova version 14.0.1. Photoluminescence data were analyzed and fit using OriginPro 2018b.

Synthesis.

The ligands and photocatalysts reported herein were synthesized by modification of previously reported procedures for tmam[32,37] and Ir-tmam.[35]

4,4'-Bis[(triethylamino)methyl]-2,2'-bipyridine Bis(hexafluorophosphate) (team). To a stirring solution of 4,4'-dibromomethyl-2,2'-bipyridine (0.200 g, 0.585 mmol) in chloroform (6 mL), triethylamine (1 mL, excess) was added. The solution was stirred for 2h at room temperature. The precipitate was filtered and washed with chloroform to give 4,4'-bis[(triethylamino)methyl]-2,2'-bipyridine dibromide. The product was dissolved in deionized (DI) water and a large excess of ammonium hexafluorophosphate was added until a precipitate formed. Collection over a fine frit, washing with DI water, and drying under vacuum gave a bright pink powder, yielding 150 mg (38%). ^{1}H NMR (400 MHz, CD_3CN) δ 8.81 (d, 2H, J = 5.0 Hz), 8.55 (s, 2H), 7.51 (dd, 2H, J = 5.0, 1.8 Hz), 4.43 (s, 4H), 3.23 (q, 12H, J = 7.2 Hz), 1.39 (t, 18H, J = 7.2 Hz). $^{13}C\{^1H\}$ NMR (151 MHz, CD_3CN) δ 156.03, 150.57, 137.12, 127.62, 124.02, 58.84, 53.14, 7.15

4,4'-Bis[(quinuclidine)methyl]-2,2'-bipyridine Bis(hexafluorophosphate) (quin). 4,4'-dibromomethyl-2,2'-bipyridine (84.6 mg, 0.247 mmol) was suspended in ethanol (~10 mL) to which a small excess of quinuclidine (96.7 mg, 0.870 mmol) was added while stirring. Addition of quinuclidine to the cloudy suspension turned the solution clear, which turned a white cloudy color again after 20 min stirring. Once the reaction proceeded for 1 h, deionized water was added dropwise until the precipitate went into solution (~0.5 mL). A saturated solution of NH_4PF_6 (aq.) was added in large excess (~2 mL), which led to immediate precipitation of the title complex. The reaction was allowed to stir for 1 h to ensure complete counterion metathesis. The precipitate was collected by vacuum filtration and washed with deionized water. The white solid was extracted into CH_3CN, dried over Na_2SO_4, then the solvent was removed in vacuo yielding 156.1 mg (91% yield). ^{1}H (400 MHz, *d*$_6$-acetone) δ 8.86 (d, 2H, *J* = 4.9 Hz), 8.66 (d, 2H, *J* = 1.6 Hz), 7.71 (dd, 2H, *J* = 5.0, 1.7 Hz), 4.76 (s, 4H), 3.81 – 3.76 (m, 12H), 2.26 (hept, 2H, *J* = 3.2 Hz), 2.15 – 2.09 (m, 12H). ^{13}C{^{1}H} NMR (151 MHz, *d*$_6$-acetone) δ 156.97, 151.22, 138.18, 129.07, 125.55, 67.13, 56.01, 24.61, 20.74.

4,4'-Bis[(phenyldimethylamino)methyl]-2,2'-bipyridine Bis(bromide) (pham). An excess of neat dimethylaniline (~0.3 mL) was added to a stirring solution of 4,4'-dibromomethyl-2,2'-bipyridine (52 mg, 0.15 mmol) dissolved in ~4 mL of acetonitrile. The solution quickly became cloudy and after stirring overnight, the milky white solution was filtered and the precipitate was collected. ^{1}H (400 MHz, *d*$_4$-methanol) δ 8.57 (dd, 2H J = 4.9, 0.8 Hz), 8.13 (dd, 2H, J = 1.7, 0.8 Hz), 7.85 – 7.80 (m, 4H), 7.67 – 7.60 (m, 6H), 7.03 (dd, 2H, J = 4.9, 1.7 Hz), 5.16 (s, 4H), 3.74 (s, 12H). ^{13}C{^{1}H} NMR (151 MHz, *d*$_6$-DMSO) δ 154.89, 159.71, 144.58, 137.97, 130.48, 130.07, 127.35, 123.96, 121.66, 69.94, 53.09.

[Ir(dF-(CF$_3$)-ppy)$_2$(tmam)][3PF$_6$] (Ir-tmam). The synthetic procedure for Ir-tmam was previously published and followed directly as reported.[35] In the preparation of this manuscript, we discovered that the original report inadvertently omitted one of the carbon resonances of Ir-tmam in the tabulated data that was observed in the ^{13}C{^{1}H} NMR spectrum. Therefore, we have included the corrected tabulated data below to clarify this error. ^{13}C{^{1}H} NMR (151 MHz, CD_3CN) 168.38 (d, *J* = 7.3 Hz), 165.45 (dd, *J* = 258.3, 12.7 Hz), 163.34 (*J* = 262.0, 13.2 Hz), 157.1, 154.58 (d, J = 7.1 Hz), 153.71, 147.19 (q, *J* = 4.8 Hz), 140.92, 138.34 (m), 133.77, 129.92, 127.81 (m), 126.49 (q, *J* = 34.4), 125.12 (d, *J* = 21.0 Hz), 123.07 (q, *J* = 271.6 Hz), 115.53 (dd, 18.5, 2.8 Hz), 100.71 (t, *J* = 28.0 Hz), 67.72, 54.22.

[Ir(dF-(CF_3)-ppy)$_2$(team)][PF_6]$_3$ (Ir-team). Synthesis was performed using an Anton Parr Monowave 300 microwave reactor. The iridium(III) chloro-bridged dimer [Ir(dF-(CF_3)-ppy)$_2$(μ-Cl)]$_2$ (20 mg, 0.013 mmol) and team (18 mg, 0.027 mmol) were suspended in 4 mL methanol in a 10 mL microwave tube. The reaction mixture was microwaved at 90°C for 1h to give a dark yellow, transparent solution. The solvent was then removed under vacuum, yielding a bright yellow solid. The solid was dissolved in ~10 mL DI water and an excess of tetrabutylammonium hexafluorophosphate was added to precipitate Ir-team as the PF_6^- salt (12 mg, 29% yield). ^{1}H NMR (500 MHz, CD_3CN) δ 8.61 (br s, 2H), 8.52 (d, 2H, *J* = 8.8, 2.5 Hz), 8.22 (dd, 2H, *J* = 8.8, 2.1 Hz), 8.12 (d, 2H, *J* = 5.6 Hz), 7.63 (dd, 2H, *J* = 5.6, 1.8 Hz), 7.58 (br s, 2H), 6.83 (ddd, 2H, *J* = 12.1, 9.3, 2.3 Hz), 5.84 (dd, 2H, *J* = 8.4, 2.3 Hz), 4.52 (s, 4H), 3.23 (q, 12H, *J* = 7.2 Hz), 1.39 (t, 18H, *J* = 7.2 Hz). ^{19}F NMR (377 MHz, CD_3CN) δ –63.3 (–CF_3), –73.0 (d, PF_6^-), –104.7 (dt, ppy–F), –107.6 (td, ppy–F). ^{13}C{^{1}H} NMR (151 MHz, CD_3CN) δ 168.38 (d, *J* = 7.5 Hz), 165.13 (dd, *J* = 260.0, 13.9 Hz), 163.60 (dd, *J* = 262.6, 14.0 Hz), 156.87, 154.57 (d, *J* = 7.4 Hz), 153.57, 147.09 (q, *J* = 4.6 Hz), 140.89, 138.32 (m), 133.45, 129.82, 127.79 (m), 126.41 (q, *J* = 34.4 Hz), 125.13 (d, *J* = 21.5 Hz), 123.04 (q, *J* = 272.2 Hz), 115.51 (dd, *J* = 18.0, 2.6 Hz), 100.68 (t, *J* = 26.9 Hz), 59.10, 54.67, 8.31. HRAM-MS (HESI) m/z calcd for $C_{48}H_{50}F_{10}IrN_6$ $[M]^{3+}$ 364.45167, found 364.45135.

[Ir(dF-(CF_3)-ppy)$_2$(quin)][3PF_6] (Ir-quin). [Ir(dF-(CF_3)-ppy)$_2$(*μ*-Cl)]$_2$ (38.4 mg, 0.026 mmol) and quin (31.8 mg, 0.046 mmol) were suspended in 8 mL of methanol in a glass microwave vial equipped with a magnetic stir bar. The reaction was microwaved at 90°C for 1h, yielding a bright yellow precipitate and yellow supernatant. The precipitate was collected by vacuum filtration and dissolved in minimal acetonitrile (~1 mL). An excess of a saturated solution of NH_4PF_6 (aq.) was added (~1 mL), followed by an additional 5 mL of deionized water, leading to precipitation of a fine yellow powder. The powder was washed with deionized water, methanol, and dichloromethane, yielding Ir-quin as the PF_6^- salt (29.4 mg, 42% yield). ^{1}H (600 MHz, CD_3CN) δ 8.55 (d, 2H, *J* = 1.7 Hz), 8.52 (dd, 2H, *J* = 8.8, 2.6 Hz), 8.23 (dd, 2H, *J* = 8.8, 2.1 Hz), 8.14 (d, 2H, *J* = 5.6 Hz), 7.65 (dd, 2H, *J* = 5.6, 1.7 Hz), 7.60 (s, 2H), 6.82 (ddd, 2H, *J* = 12.2, 9.6, 2.3 Hz), 5.82 (dd, 2H, *J* = 8.4, 2.3 Hz), 4.44 (s, 4H), 3.43 (app t, 12H, *J* = 7.8 Hz), 2.18 (hept, 2H, *J* = 3.2 Hz), 1.98 – 1.93 (m, 12H). ^{13}C{^{1}H} NMR (151 MHz, CD_3CN) δ 168.47 (d, *J* = 6.7 Hz), 165.51 (dd, *J* = 258.5, 12.5 Hz), 163.40 (dd, *J* = 261.6, 13.1 Hz), 156.95, 154.68 (d, *J* = 7.3 Hz), 153.47, 147.08 (q, *J* = 4.7 Hz), 140.83, 138.41 – 138.33 (m), 133.96, 130.22, 127.86 – 127.79 (m),

126.52 (q, J = 33.0 Hz), 125.16 (d, J = 20.8 Hz), 123.10 (q, J = 271.8 Hz), 115.53 (dd, J = 18.2, 2.6 Hz), 100.74 (t, J = 27.1 Hz), 66.11, 56.54, 24.38, 20.40. ^{19}F (377 MHz, CD_3CN) δ –63.3 (s, –CF_3), –72.6 (d, PF_6^-, J = 707.1 Hz), –104.8 (dt, ppy–F, J = 12.4, 8.4 Hz), –107.7 (td, ppy–F, J = 12.4, 12.2, 2.7 Hz). ^{31}P NMR (243 MHz, CD_3CN) δ –144.6 (hept, PF_6^-, J = 707.1 Hz). HRAM-MS (HESI) m/z calcd for $C_{50}H_{46}F_{10}IrN_6$ $[M]^{3+}$ 371.10790, found 371.10808.

[Ir(dF-(CF$_3$)-ppy)$_2$(pham)][3PF$_6$] (Ir-pham). [Ir(dF-(CF$_3$)-ppy)$_2$(μ-Cl)]$_2$ (75 mg, 0.0504 mmol), pham (58.88 mg, 0.1008 mmol), and silver nitrate (25.7 mg, 0.151 mmol) were suspending in 5 mL of methanol in a 10 mL Anton-Parr microwave reactor vial equipped with a magnetic stir bar. The suspension was microwaved for 1 h at 90°C, resulting in a yellow solution and an off-white precipitate that was filtered through off through a plug of celite. An excess of sat. NH_4PF_6 (~5 mL) was added to the solution, which initially turned cloudy and then returned to a translucent yellow color. The product was then precipitated out of solution with excess DI water. The precipitate was collected and recrystallized from THF:H_2O by vapor diffusion, yielding Ir-pham as the PF_6^- salt (50 mg, 63% yield). ^{1}H NMR (500 MHz, CD_3CN) δ 8.48 (dd, J = 9.31, 2.1 Hz, 2H), 8.22 (dd, J = 9, 1.74 Hz, 2H), 7.92 (d, J = 5.7 Hz, 2H), 7.87 (s, 2H), 7.26 (m, 10H), 7.48 (s, 2H), 7.06 (dd, J = 5.72, 1.78 Hz, 2H), 6.79 (ddd, J = 12.07, 9.26, 2.3 Hz, 2H), 5.76 (dd, 8.44, 2.3 Hz, 2H), 4.97 (d, J = 1.88 Hz, 4H), 3.62 (s, 12H). ^{19}F NMR (377 MHz, CD_3CN) δ –63.17 (–CF3), –73.71 (d, PF_6), –104.7 (dt, ppy–F), –107.7 (td, ppy–F).^{13}C{^{1}H} NMR (101 MHz, CD_3CN) δ 168.22 (d, J = 7.34 Hz), 165.59 (dd, J = 208.46, 12.48 Hz), 163.02 (dd, J = 213.52, 15.85 Hz), 156.41, 154.22 (d, J = 7.22 Hz), 152.93, 146.99 (q, J = 4.83 Hz), 144.45, 140.78, 138.3 (m), 132.99, 132.27, 131.69, 129.27, 127.64 (m), 126.41 (q, J = 34.41 Hz), 125.05 (d, J = 21.27 Hz), 123.01 (q, J = 271.43 Hz), 121.89, 115.45 (dd, 18.07, 2.86 Hz), 100.64 (t, 27.15 Hz), 71.25, 55.07*, 54.64*. *The noted resonances arise from asymmetric methyl groups. HRAM-MS (HESI) *m/z* calcd for $C_{52}H_{42}F_{22}IrN_6P_2$ $[M]^+$ 1423.221, found 1423.223; *m/z* calcd for $C_{52}H_{42}F_{16}IrN_6P$ $[M]^{2+}$ 639.128, found 639.129.

RESULTS

A series of bipyridyl ligands featuring two pendant ammonium groups were synthesized by procedures adapted from prior literature following the general scheme shown in **Figure 1**. Reaction of these ligands with the iridium(III) chloro-bridged dimer, [Ir(dF-(CF$_3$)-ppy)$_2$(μ-Cl)]$_2$,

followed by salt metathesis yielded the structurally related series of iridium photocatalysts shown in **Figure 2**.

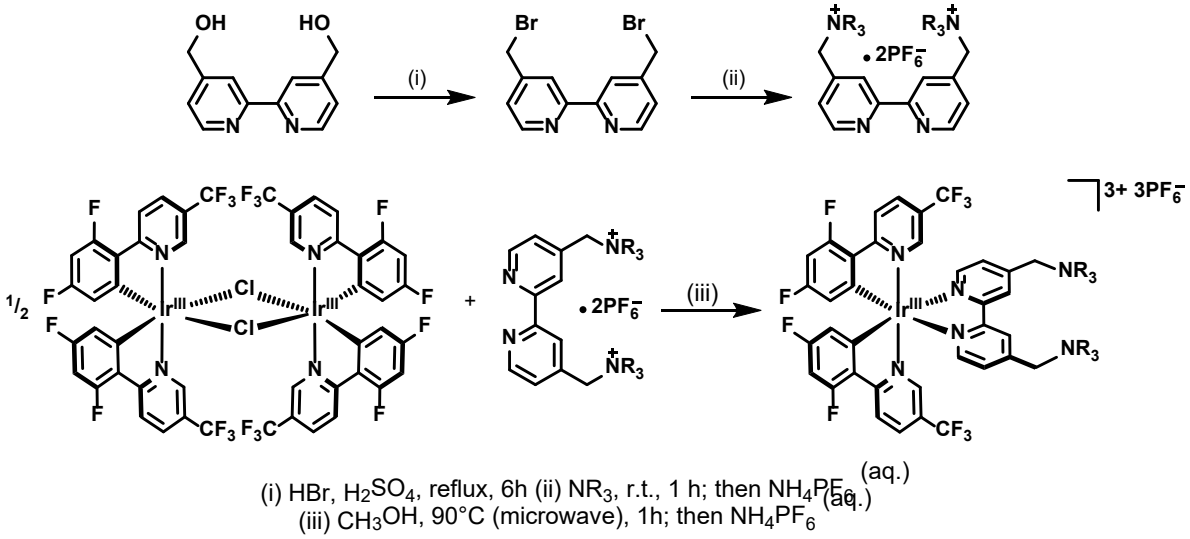

Figure 1. Generic synthetic scheme for ligands and photocatalysts.

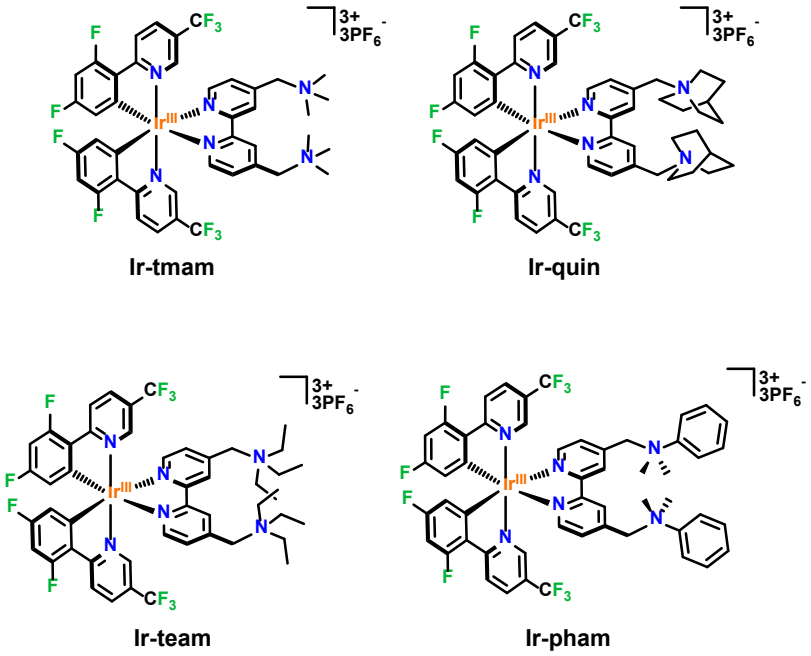

Figure 2. Series of Ir photocatalysts with pendant quaternary ammonium ligands and their abbreviated names.

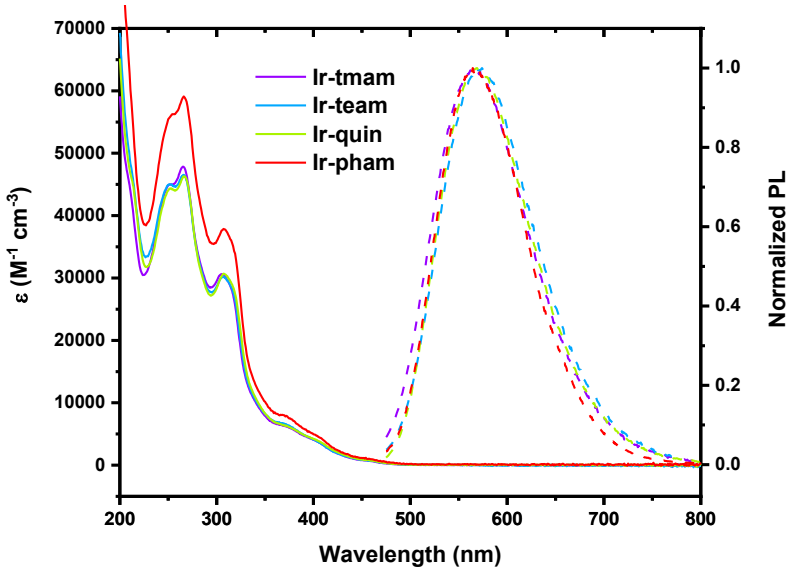

Figure 3. Molar extinction (solid) and normalized photoluminescence (dashed) of the Ir photocatalysts.

The absorbance profiles shown in **Figure 3** were quite similar across the series of PCs with absorbances tailing into the blue edge of the visible region and two intense features in the UV region.[42,43] Visible-light excitation resulted in broad photoluminescence (PL) bands centered around ~570 nm. Pulsed-light excitation created PL decays that were well described by a first-order kinetic model from which the excited-state lifetimes, τ_0, were extracted. In electrochemical experiments, the first reduction peak for iridium photocatalysts containing one bipyridyl-type ligand and two cyclometallating phenylpyridine (ppy) ligands has been assigned to occur at the bipyridine ligand. For these complexes, irreversible reductions were observed near $E°'(Ir^{3+/2+}) \approx -1.3$ V vs $Fc^{+/0}$ (estimated from half cathodic peak height) in acetonitrile electrolyte solutions. Irreversible features have been reported for related complexes bearing benzylic quaternary ammonium substituents, which has been attributed to the cleavage of the C–N bond and displacement of the amine.[32,35,44–46] The free energies stored in the excited state, ΔG_{es}, were extracted from the blue edge of the PL spectrum and used in conjunction with **Equation 1** to estimate the excited-state reduction potentials given in **Table 1**.

$$E°'(Ir^{3+*/2+}) = E°'(Ir^{3+/2+}) + \Delta G_{es} \qquad \textbf{Equation 1}$$

Table 1. Excited-state lifetimes (τ_0), photoluminescence maxima, and ground- and excited-state reduction potentials for Ir photocatalysts.

	τ_0 (ns)	ΔG_{es} (eV)	PL_{max} (nm)	$E°'([Ir]^{3+/2+})$ (V vs $Fc^{+/0}$)	$E°'([Ir]^{3+*/2+})$ (V vs $Fc^{+/0}$)
Ir-tmam	1000	2.55[a]	567	-1.32[a]	1.23[a]
Ir-team	950	2.53	572	-1.30	1.23
Ir-quin	900	2.52	569	-1.31	1.21
Ir-pham	550	2.52	567	-1.29	1.23

[a]Value reported in Ref. 35.

The ^{1}H and ^{13}C NMR spectroscopic data were utilized to characterize the catalysts in CD_3CN solutions. For Ir-tmam, Ir-team, and Ir-quin, the ^{1}H chemical shifts appeared in the same relative positions for corresponding hydrogen atoms with only minor variations observed in their absolute positions, Figure S7, Figure S9, and Figure S11, respectively. For Ir-pham, both the 3,3' and 5,5' hydrogens of the bipyridyl ligand were significantly more shielded than for the other PCs, Figure S14.

Chloride titration studies with a ^{1}H NMR assay studies were used to determine the location and binding affinity of chloride to the iridium photocatalysts. Addition of TBACl to CD_3CN solutions of the iridium complexes showed qualitatively similar behavior across the series with representative data for Ir-quin shown in **Figure 4**. The most pronounced changes in chemical shift occurred for the 3,3' hydrogen atoms of the bipyridyl-type ligand (labeled "h" in **Figure 4**). For Ir-tmam, Ir-team, and Ir-quin, the 5,5' hydrogen resonances labeled "g" shifted slightly upfield at low chloride concentrations and then shifted downfield when additional equivalents were added, Figure S17, Figure S18, and **Figure 4**, respectively. The inflections observed in these changes in chemical shifts are consistent with a secondary chloride binding event at superstoichiometric concentrations. Additional chemical shift changes were observed for the hydrogens located in the α-positions relative to the ammonium nitrogen (labeled "i" and "j") that shifted more gradually than the 3,3' hydrogens, consistent with weaker binding of a second chloride ion. For Ir-pham, the 5,5' hydrogens (labeled "g") as well as those labeled "i" and "j" exhibited a gradual downfield shift across all chloride concentrations, also consistent with 1:2 (photocatalyst/chloride) binding. The chemical shifts were fit as a function of chloride concentration using a 1:2 binding model to calculate the equilibrium constants for ion pairing.[40,41,47] Despite the qualitatively similar chemical shift changes observed across the series, the equilibrium constants tabulated in **Table 2** indicate a pronounced difference in binding affinity depending on the identity of the pendant group attached

to the bipyridyl ligand. The largest affinity for chloride binding was observed for Ir-pham with K_{11} = 4.7 ± 1.7 x10^5 M^{-1} and the smallest for Ir-quin with K_{11} = 1.8 ± 0.13 x10^4 M^{-1}.

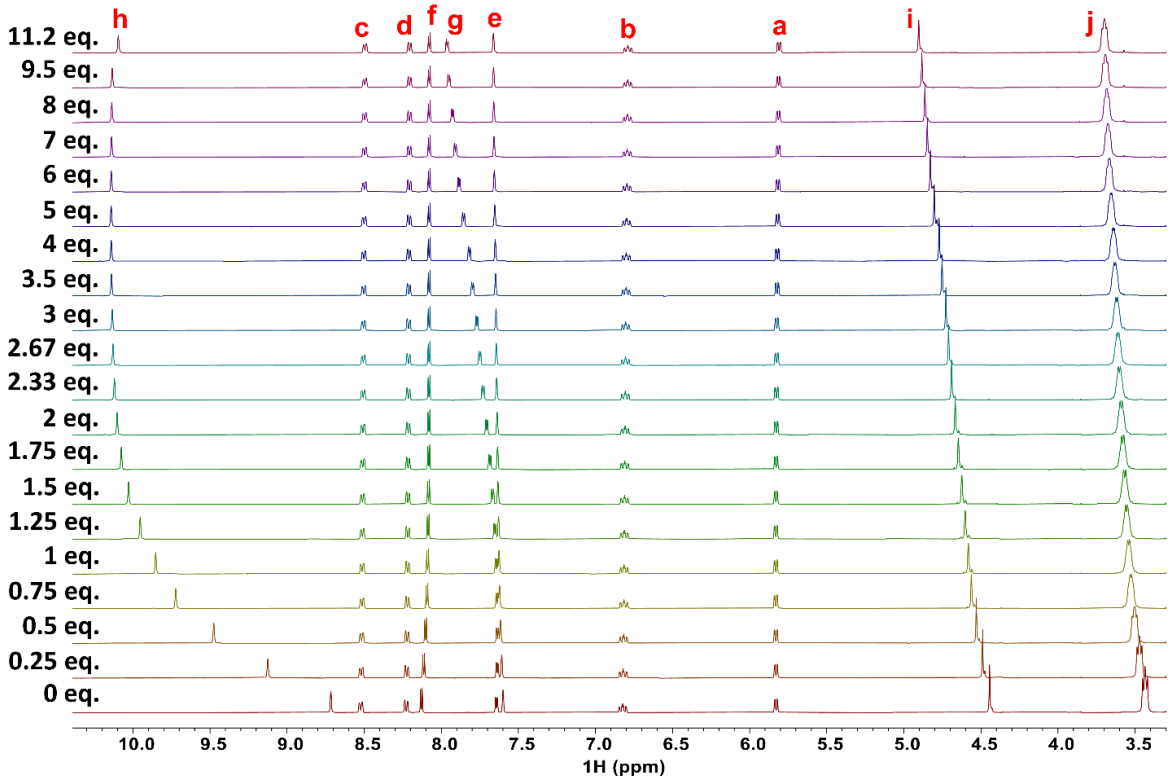

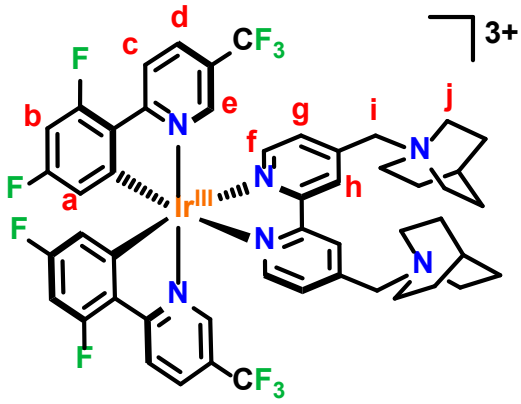

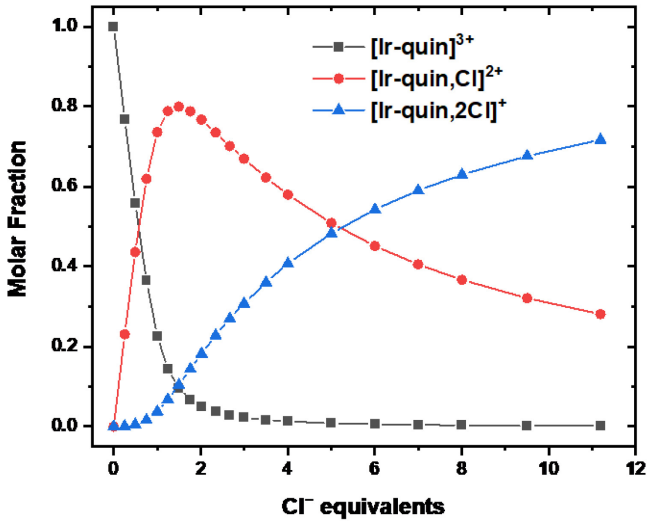

Figure 4. ^{1}H NMR of Ir-quin in CD_3CN with TBACl titrated from 0 to 11.2 equivalents. Molar fraction plot of ion-paired Ir-quin as a function of chloride concentration.

Table 2. Equilibrium constants for chloride binding to the corresponding Ir photocatalyst in CD_3CN determined from ^1H NMR titrations.

	K_{11} (M^{-1})	K_{12} (M^{-1})
Ir-tmam	$3.7 \pm 0.7 \times 10^5$	$1.1 \pm 0.07 \times 10^3$
Ir-team	$8.1 \pm 3.0 \times 10^4$	$3.5 \pm 1.1 \times 10^2$
Ir-quin	$1.8 \pm 0.13 \times 10^4$	$2.7 \pm 0.12 \times 10^2$
Ir-pham	$4.7 \pm 1.7 \times 10^5$	$2.9 \pm 0.6 \times 10^3$

In addition to the chemical shift changes in the presence of chloride, subtle breaks in symmetry were observed that provided a glimpse toward unique ion-paired solution structures for each photocatalyst. The methylene hydrogens on the sp^3 carbons that connect the quaternary ammonium groups to the bipyridyl ligand (labeled "i") appeared as singlets for all photocatalysts in the absence of chloride. For Ir-tmam and Ir-team, however, spectra acquired at and proximate to 1 equivalent of chloride exhibited splitting of these hydrogen resonances into strongly coupled roofed doublets that was not observed for the other two photocatalysts, Figure S17 and Figure S18, respectively. Interestingly, there was no indication that the degeneracy of other hydrogen resonances was broken because the C_2 symmetry axis that bisects the bipyridyl ligand and the metal center for Ir-tmam and Ir-team at these chloride concentrations was maintained. By 2 equivalents of chloride, the methylene resonances re-converged into a singlet for both PCs. Remarkably, the methylene resonances for Ir-team split again around 5 equivalents of chloride, which coincided with where the doubly ion-paired photocatalyst, $[Ir\text{-}team,2Cl]^+$, became the predominant species in solution.

For Ir-pham, the $N–(C\boldsymbol{H}_3)_2$ methyl hydrogens that appeared as a chemically equivalent singlet in absence of chloride split into two chemically inequivalent singlets in the presence of chloride at all concentrations studied, Figure S19. The difference in their chemical shifts increased with chloride concentration up to 1 equivalent, coinciding with the concentration where essentially no "free" $[Ir\text{-}pham]^{3+}$ remained, after which point no change in the 0.04 ppm peak separation was observed. Similar to that described above, there was no indication of a loss of C_2 symmetry for any other hydrogen resonances.

Steady-state PL titrations revealed a blue shift in the PL_{max} with increasing chloride concentration. For example, a blue shift of ~9 nm was observed for Ir-tmam by 1.5 equivalents of

chloride added *i.e.*, where the concentration of the singly ion-paired complex, [Ir-tmam,Cl]$^{2+}$, was greatest, Figure S20. Additional chloride up to 25 equivalents continued to blue shift the PL, albeit to a lesser extent than the first chloride-binding event.

Time-resolved PL decays recorded after 460 nm pulsed-light excitation were mono-exponential with lifetimes around 1 μs (550 ns for Ir-pham) in argon-purged acetonitrile solutions, **Table 1**. Titration of chloride led to quenching of the excited-state photocatalyst lifetimes. Representative data is shown in **Figure 5** for Ir-quin, but the observations henceforth were common for each photocatalyst, shown in Figures S21-S23, unless otherwise noted. Interestingly, the quenching behavior was dependent on the monitoring wavelength. Monitoring the time-resolved PL decay on the red edge of the broad PL feature (650 nm) displayed monoexponential decay kinetics (**Equation 2**) with a first-order dependence on the chloride concentration, **Figure 5a**.

$$PLI(t) = \alpha(\exp(-t/\tau)) \qquad \textbf{Equation 2}$$

This behavior was consistent with a diffusional or dynamic quenching model. The lifetimes as a function of chloride concentration were satisfactorily fit to the Stern–Volmer Relationship (**Equation 3**) to determine the rate constants for dynamic quenching.

$$\frac{\tau_0}{\tau} = 1 + \tau_0 k_\mathrm{q}[\mathrm{Q}] \qquad \textbf{Equation 3}$$

Interestingly, monitoring the time-resolved PL on the blue edge of the PL (540 nm) displayed kinetics that were best described by a biexponential kinetic model (**Equation 4**), indicative of two distinct quenching pathways, **Figure 5b**.

$$PLI(t) = \alpha_1\left(exp\left(-\frac{t}{\tau}\right)\right) + \alpha_2\left(exp\left(-\frac{t}{\tau_s}\right)\right) \qquad \textbf{Equation 4}$$

One quenching pathway exhibited a lifetime with a first-order dependence on the chloride concentration, consistent with a diffusional quenching mechanism. The quenching rate constant was in good agreement with that extracted from kinetic data acquired at longer monitoring wavelengths. The second lifetime, τ_s, was independent of the chloride concentration and was only observed once chloride was in solution. This second quenching pathway is consistent with a unimolecular or "intra-ionic" process where the photocatalyst was quenched by the chloride that was pre-associated in the ground state—a process known as static quenching. The rate constants

for both quenching processes are tabulated in **Table 3** for each photocatalyst. The diffusional quenching rate constants for each photocatalyst were all between $3 - 4 \times 10^{10}$ M^{-1} s^{-1} and differed by less 20%. In contrast, the rate constants for intra-ionic quenching varied by a factor of 3 between photocatalysts. Note that the rate constant for static quenching is reported as an electron transfer rate constant, $k_{et} = 1/\tau_s$, because this quenching does not involve diffusion.

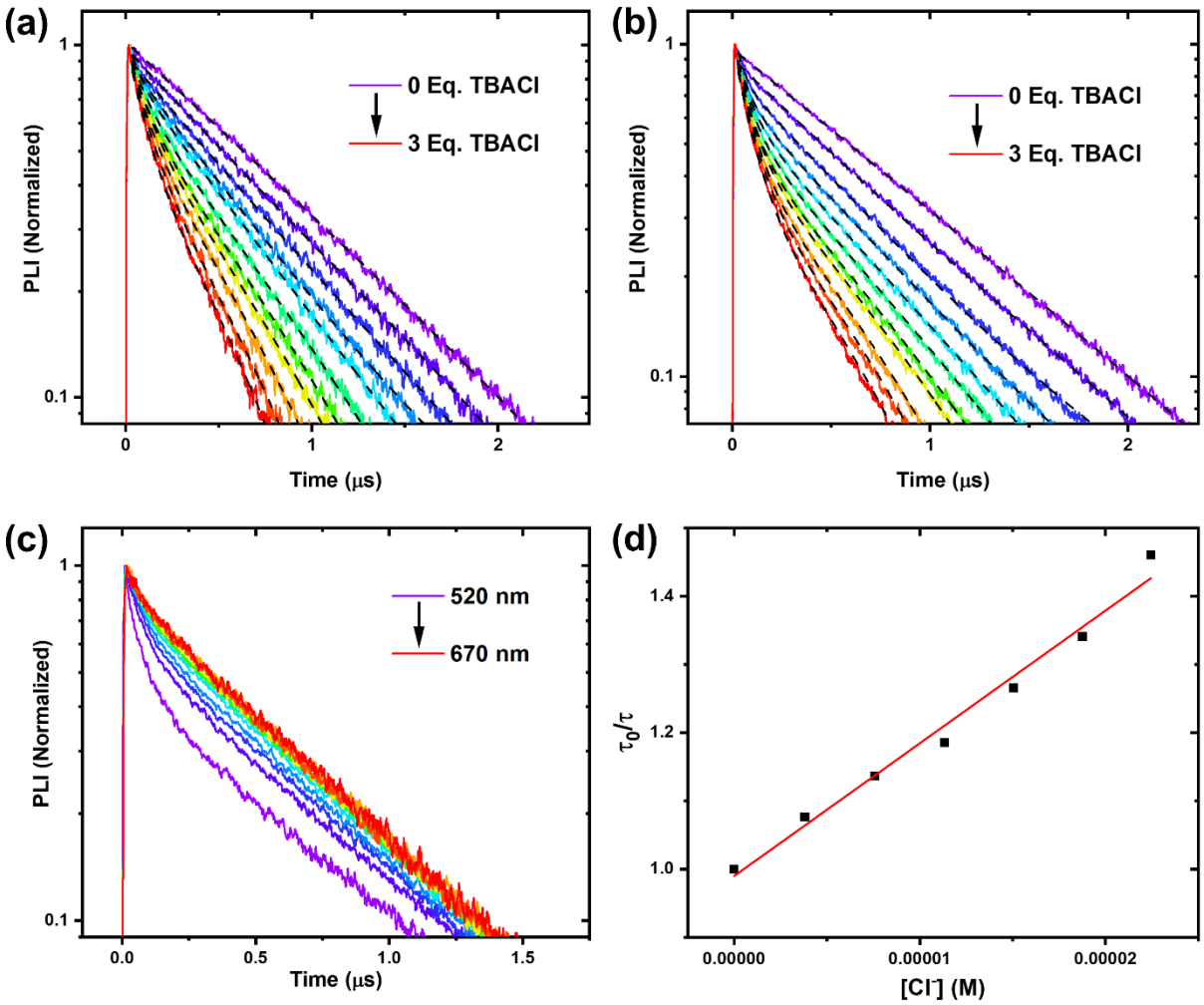

Figure 5. Time-resolved PL of Ir-quin upon titration of TBACl monitored at 650 nm (a) and 540 nm (b) wavelengths. Panel (c) shows the time-resolved PL of Ir-quin in the presence of 1 equivalent of TBACl monitored from 520 nm (purple) to 670 nm (red) wavelength region. (d) Stern–Volmer plot for diffusional quenching mechanism.

Table 3. Rate constants for diffusional and intra-ionic quenching processes.

	k_q (M^{-1} s^{-1})	τ_s (ns)	k_{et} (static) (s^{-1})
Ir-tmam	3.1×10^{10}	92	1.1×10^{7}
Ir-team	3.1×10^{10}	53	2.3×10^{7}
Ir-quin	3.4×10^{10}	65	1.6×10^{7}
Ir-pham	3.8×10^{10}	120	8.3×10^{6}

Time-resolved PL measurements of chloride titrations performed in the presence of 0.1 M $TBAPF_6$ as a supporting electrolyte yielded monoexponential decay kinetics at all monitoring wavelengths with a first-order dependence on chloride concentration, **Figure 6**. Charge screening in high ionic strength solutions is expected to attenuate Coulombic attraction and thus greatly diminish ion pairing between chloride ions and the photocatalysts.[48] Thus, the absence of the additional quenching mechanism in acetonitrile solutions containing 0.1 M $TBAPF_6$ supports the assignment of an intra-ionic quenching pathway.

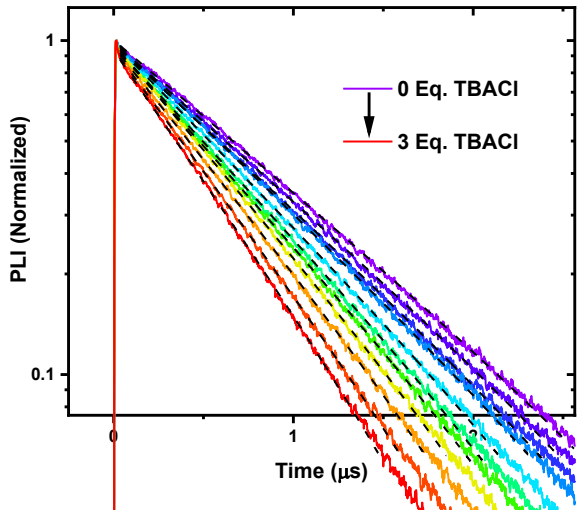

Figure 6. Time-resolved photoluminescence of Ir-quin monitored at 540 nm in a 0.1 M $TBAPF_6$ acetonitrile solution with 0 to 3 equivalents of chloride.

As a comparative control, iridium photocatalysts with the same cyclometallating ligands that lack the quaternary amine groups on the bipyridyl ligands were investigated in CH_3CN. When

illuminated with visible light, the commercially available parent bpy complex, $[Ir(dF\text{-}(CF_3)\text{-}ppy)_2(bpy)]^+$ was quenched by Cl^- in agreement with the Stern-Volmer model, $k_q = 8.6 \times 10^7\ M^{-1}\ s^{-1}$, Figure S24. The corresponding 4,4'-(*tert*-butyl)$_2$-bpy complex $[Ir(dF\text{-}(CF_3)\text{-}ppy)_2(dtb)]^+$ showed negligibly small quenching behavior that is consistent with a previous report.[7] The analogous 4,4' and 5,5' bis-CF_3 bipyridine photocatalysts, $[Ir(dF\text{-}(CF_3)\text{-}ppy)_2(4,4'\text{-}(CF_3)_2\text{-}bpy)]^+$ and $[Ir(dF\text{-}(CF_3)\text{-}ppy)_2(5,5'\text{-}(CF_3)_2\text{-}bpy)]^+$, were far more effective for chloride oxidation with $k_q = 9.1 \times 10^9\ M^{-1}\ s^{-1}$ and $8.4 \times 10^9\ M^{-1}\ s^{-1}$, respectively.[43] Importantly, a solely dynamic quenching mechanism was evident for the photocatalysts where significant chloride quenching was observed with no evidence for the bi-exponential kinetics and static electron transfer assigned to chloride association with the quaternary amine cations herein.

DISCUSSION

A new series of iridium photocatalysts was synthesized and characterized for photo-induced halide oxidation. The dicationic ligands—team, tmam, pham, and quin—bearing positively charged alkyl and/or aryl ammonium groups provided favorable electrostatic interactions that pre-associated chlorides with the photocatalysts even in highly polar acetonitrile solutions. The excited-state properties of the Ir photocatalysts shown in **Figure 2** were remarkably insensitive to variation of the cationic ammonium groups linked to a common bipyridyl ligand. However, chloride titration studies with a ^1H NMR assay revealed subtle, yet significant differences in the average solution structures and equilibrium constants for chloride association. Below, we discuss the solution structures inferred from spectroscopic data followed by a description of the excited state reaction chemistry.

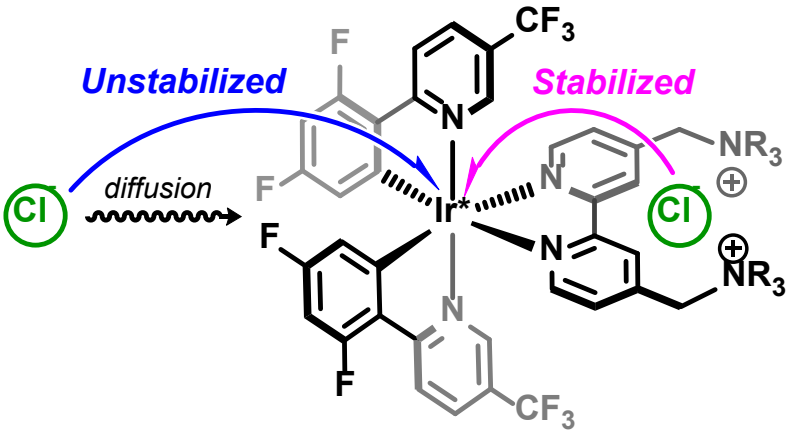

Figure 7. Schematic of chloride ion pairing within the photocatalyst binding pocket and the two competitive electron transfer processes.

Solution Structure and Chloride Ion Pairing.

Compelling evidence for ion-pair formation between chloride and the photocatalysts was observed from NMR and photoluminescence spectroscopies. The blueshift in the PL spectra of the PCs upon chloride addition provided indirect evidence for ion pairing. In addition, the significant downfield shifts of resonances assigned to the 3 and 3' protons on the bipyridyl-type ligands upon increasing chloride concentration indicated that these ligands act as a "binding pocket" for the chloride ion, **Figure 7**. Previous studies with ruthenium and iridium photocatalysts capable of forming ion pairs with halides have attributed this behavior to H-bonding interactions between the most electrophilic H atoms on the bipyridyl ligand and the electronegative halide ion, which results in deshielding and a downfield shift of these resonances.[32,35,49,50] A weaker secondary chloride binding interaction was indicated by additional chemical shift changes that occurred at superstoichiometric chloride concentrations, consistent with similar previously reported complexes.[35,48,50]

Comparison of the spectral changes observed in the ^{1}H NMR titration studies revealed subtle differences between the photocatalysts that provided greater insight into the structures of the ion pair in solution than had been realized in prior studies. The methylene hydrogens proximal to the ammonium substituents (drawn in purple in **Figure 4.8**) are rigorously classified as diastereotopic environments, yet appear as a chemically-equivalent singlet in the absence of chloride for all the complexes described herein. For Ir-tmam and Ir-team, however, this resonance splits into strongly coupled roofed doublets at chloride concentrations near 1 equivalent. We attribute this observation to greater inequivalence of the adjacent methylene hydrogen atoms upon chloride binding due to preferential orientation of the ammonium substituents above and below the plane of the bipyridyl ligand. Partially restricted rotation about the pyridyl *ipso*-C–C(H_2) bonds (maroon arrow in **Figure 8**) resulting from the ion-paired chloride is consistent with distinct pseudo axial and equatorial hydrogen environments for the methylene linker that still maintains the observed C_2 symmetry for the rest of the equivalent hydrogen resonances in Ir-tmam and Ir-team.

For Ir-pham, the methylene hydrogens appeared chemically equivalent in the presence of chloride, but inequivalence was observed for the N–(C***H***$_3$)$_2$ hydrogens at all (nonzero) chloride concentrations investigated. Here, we postulate that the different chemical environments arise from the methyl groups (drawn in Carolina blue in **Figure 8**) pointed inward toward the ion-paired chloride versus outward toward the surrounding. Note that this asymmetry results from partially restricted rotation around the C(H$_2$)–N bond (red arrow in **Figure 8**), as opposed to that described for Ir-tmam/Ir-team.

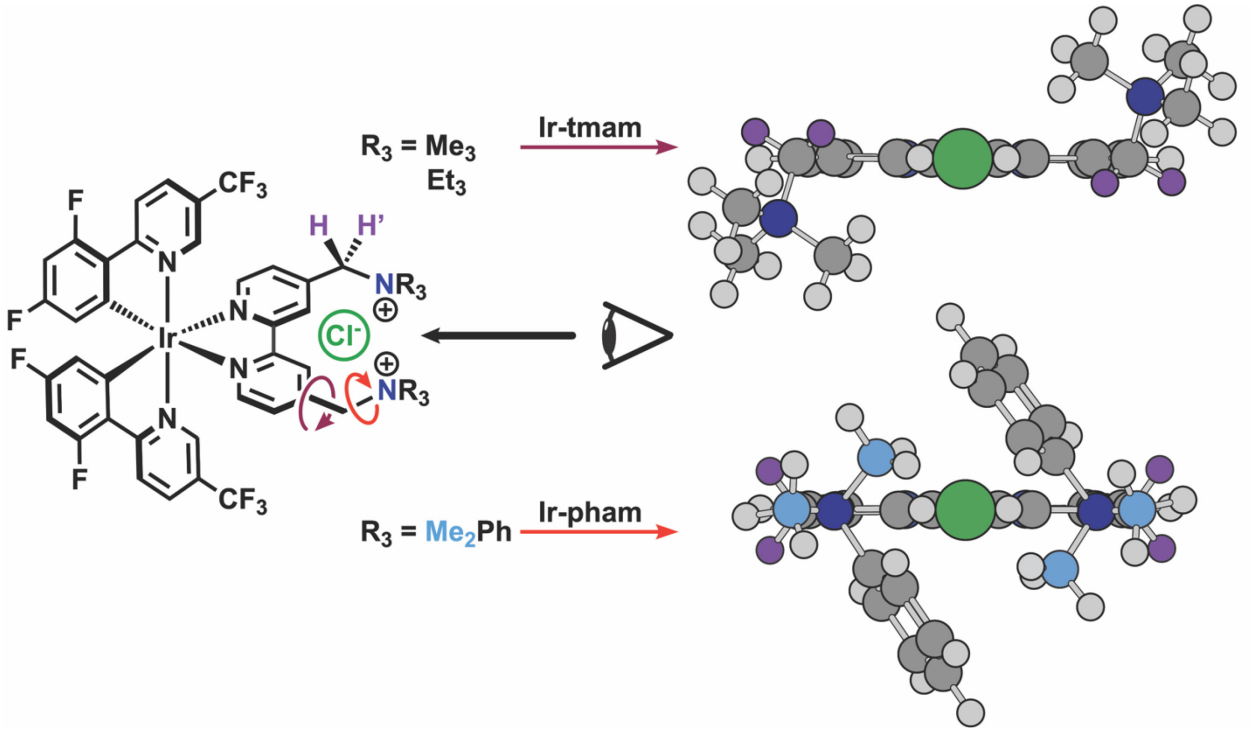

Figure 8. Proposed solution structures for Ir-tmam/Ir-team (top) and Ir-pham (bottom) upon chloride ion pairing with the relevant bond rotations from planarity indicated on the right (in red and maroon, respectively). These illustrations are not intended to indicate that these complexes are conformationally locked in the geometry depicted, but rather to represent plausible predominant rotamers that account for the asymmetry observed by NMR in the presence of chloride.

For Ir-quin, a subtle change in the splitting pattern was observed for the quinuclidine hydrogens in the α-position relative to the quaternary nitrogen at various chloride concentrations, but this change did not provide any structural insight. The lack of clear structural change upon chloride binding is consistent with a weaker interaction with the chloride ion that is reinforced by the larger steric encumbrance at the cationic nitrogen moieties. Indeed, the equilibrium constant

for chloride binding (K_{11}) for Ir-quin was least favorable and nearly a factor of 5 smaller than the next lowest equilibrium constant for the series of photocatalysts reported herein.

The largest chloride equilibrium association constants were observed for Ir-pham, K_{11} = 4.7 ± 1.7 x10^5 M^{-1}, and Ir-tmam, K_{11} = 3.7 ± 0.7 x10^5 M^{-1}. Although these two equilibrium constants were the same within experimental uncertainty, their relative magnitudes were somewhat unexpected based on the additional steric encumbrance of a phenyl substituent relative to a methyl group. However, a longstanding and growing body of literature suggests the possibility for constructive anion−π interactions, particularly for electron-deficient arenes.[51] Ir-team displayed approximately a factor of 5 smaller binding affinity for chloride than Ir-tmam, affirming the intuitive conjecture that small changes in steric bulk on the cationic ammonium groups dramatically affect the magnitude of ion pairing.

Excited State Reaction Chemistry.

All of the Ir photocatalysts displayed long-lived photoluminescent excited states and remarkably similar excited-state reduction potentials (the variation was less than k_BT). The presence of chloride ions resulted in two distinct quenching pathways. Kinetic data from time-resolved photoluminescence experiments performed in the presence of chloride showed that excited-state decay was non-exponential and well described by a biexponential function. One process was independent of [Cl^-], while the other was first-order in [Cl^-] concentration. The former process was attributed to "static" electron transfer from the ion-paired chloride, while the second process was attributed to "dynamic" or diffusional electron transfer with freely diffusing chloride ions, **Figure 7**. Importantly, the static reaction occurs "intra-ionically" and hence does not require diffusion of chloride, enabling excited-state electron transfer on a nanosecond time scale. Control experiments with bipyridine ligands that did not contain the quaternary amines showed single exponential kinetics in CH_3CN at all chloride concentration investigated, behavior that is consistent with a solely dynamic quenching mechanism.

We note that textbook definitions of "static quenching" depict the photocatalyst as a completely non-luminescent adduct with the quencher.[33] However, this need not be the case. Electron transfer may be kinetically competitive with radiative relaxation for a variety of reasons such as a low driving force for electron transfer. Indeed, recently reported photocatalysts ion paired with iodide or bromide ions were found to be photoluminescent.[35] Here, we have shown that this behavior can be extended to the much more challenging to oxidize chloride ion and that this

phenomenon of time-resolved static quenching from ion-paired quenchers is generalizable to a series of iridium photocatalysts that bear pendant cationic ammonium groups.

A convenient method for quantifying the two quenching processes exploited the blue shift in the PL spectra that accompanied chloride association; time-resolved PL decays monitored on the red edge of the photocatalysts' emission were first-order with evidence for only dynamic quenching. In contrast, time-resolved PL decays monitored on the blue edge of the PL displayed biexponential decay kinetics attributed to competitive dynamic and static quenching mechanisms. The presence of static quenching only on the high energy side of the emission is consistent with the blueshift in the PL spectra measured during chloride titration studies indicating that the that the ion-paired $[Ir,Cl]^{2+*}$ photocatalysts emit light at higher energy. Thus, kinetics measurements made by monitoring the lower energy side of the PL report solely on diffusional quenching of the free $[Ir]^{3+}$ photocatalyst, whereas measurements of the shorter wavelengths report on competitive quenching between diffusional quenching of $[Ir]^{3+}$ and static quenching of $[Ir,Cl]^{2+}$.

The rate constants for dynamic quenching by chloride were within 20% across the series of photocatalysts. The similar quenching rate constants are consistent with a comparable driving force for oxidation of halides freely diffusing in solution due to the remarkably similar excited-state reduction potentials for the photocatalyst series. Interestingly, the quenching rate constant for the ion-paired chloride (or equivalently, the electron transfer rate constant for this unimolecular process, $k_{et} = k_q = 1/\tau_s$) showed a significantly more pronounced dependence on the photocatalyst identity, with nearly a threefold difference across the series.

We initially hypothesized that the photocatalyst with the largest equilibrium constant for chloride binding would exhibit the smallest rate constant for oxidation of the ion-paired chloride. This supposition was based on the anticipation that the highest binding affinity would provide the greatest stabilization to the chloride anion and thus make the halide more challenging to oxidize.[34] Indeed, the Ir-pham photocatalyst exhibited the largest equilibrium constant for ion pairing and the smallest rate constant for oxidation of the ion-paired chloride. The Ir-tmam photocatalyst similarly followed this trend, but an unexpected reversal was observed for Ir-quin and Ir-team, where the former had the smallest binding equilibrium constant but the latter had the largest rate constant for intra-ionic chloride oxidation.

As electron transfer is highly sensitive to distance, small structural changes may result in significantly different rate constants. The sp^3 hybridized methylene carbons that separate the

cationic sites from the bipyridyl ligand may allow the chloride ion to adopt a range of orientations. Indeed, the ^{1}H NMR titration data indicate subtle yet important solution structure differences unique to each photocatalyst. In principle, a more structurally homologous series of photocatalysts could be achieved with rigid spacers that provide less conformational flexibility of the ion-pairing group(s), and thus, the chloride ion. However, rigid spacers like those based on aromatic or olefin groups are also likely to impact the excited state behavior of the photocatalyst, thereby complicating comparative analysis. For the photocatalysts reported here, a qualitative comparison of the equilibrium constants and the first-order electron transfer rate constants reveals a more nuanced relationship between ion pairing and stabilization of the chloride ion toward oxidation than what can be predicted by binding affinity alone.

CONCLUSION

A new family of Ir photocatalysts bearing a series of ligands containing pendant cationic substituents was synthesized and characterized for their ability to promote ion pairing with chloride. The identity of the quaternary ammonium group had negligible impact on the intrinsic photophysical properties of the photocatalysts, but was shown to have over an order of magnitude influence on the binding affinity for chloride ions. The ability to tune interactions with redox-active ions in the secondary coordination sphere independently of the excited-state properties of the photocatalyst has significant implications for solar energy and photoredox applications.

By promoting ground-state association of chloride with these photocatalysts, intra-ionic chloride oxidation was achieved on a rapid, nanosecond timescale. Examples of light-initiated chloride oxidation are growing, but remain uncommon due to the challenging thermodynamics compared to the other halogen congeners. Prior studies have shown that ion-pairing interactions generate stabilized halide ions that are more challenging to oxidize; thus, intra-ionic oxidation of chloride, which has the greatest utility in practical synthetic applications,[5] is a significant step forward.

The relationship between chloride ion binding affinities and the rate constants for oxidizing the ion-paired chlorides was explored. The data revealed that while there is likely an inverse correlation between these parameters as one would intuitively predict, a more nuanced understanding of the ion-pair structure is necessary to fully rationalize the relationship between ion stabilization and electron transfer kinetics. Indeed, ^{1}H NMR titration studies provided evidence

for subtle differences in the average solution structure for ion pairs formed between chloride and the photocatalysts described herein.

Instances of chloride oxidation by visible light are rare.[7,26,43,52–54] Nevertheless, chloride is naturally abundant in comparison to the other halides and is of particular interest for future solar energy applications. While there are a select number of photocatalysts capable of oxidizing chloride in solution, the formation of ion pairs with the Ir photocatalysts reported here enabled rapid excited-state electron transfer at extremely low concentrations of chloride. This result is compelling for further mechanistic studies on related photocatalysts and is especially relevant to solar energy development. The ability to time resolve excited-state electron transfers that occur from adducts that are formed in the ground state whose solution structures can be probed using routine spectroscopic measurements offers new frontiers toward understanding the factors that influence electron transfer kinetics. With the recent push toward using more earth-abundant first row metal and organic photocatalysts that generally suffer from short-excited state lifetimes, new insights into the influence of pre-associating substrates to bypass diffusional constraints on excited-state reactivity holds great promise for applications beyond the Ir photocatalysts presented here.

ACKNOWLEDGMENT

The research was supported by the National Science Foundation under Award CHE-1465060. A.M.D acknowledges the Department of Chemistry at the University of North Carolina for providing individual funding through the Eliel Fellowship.

ASSOCIATED CONTENT

Supporting Information. The Supporting Information is available free of charge on the ACS Publications website.

^{1}H, ^{13}C, and ^{19}F NMR characterization of ligands and photocatalysts; ^{1}H NMR chloride binding titration experiments; steady-state and time-resolved photoluminescence for chloride titrations and associated Stern-Volmer analysis.

AUTHOR INFORMATION

Corresponding Author

gjmeyer@email.unc.edu

Notes

The authors declare no competing financial interests.

REFERENCES

(1) Troian-Gautier, L.; Turlington, M. D.; Wehlin, S. A. M.; Maurer, A. B.; Brady, M. D.; Swords, W. B.; Meyer, G. J. Halide Photoredox Chemistry. *Chem. Rev.* **2019**, *119* (7), 4628–4683.

(2) Gutmann, V. *Halogen Chemistry*, 1st ed.; Elsevier, 1967.

(3) Liu, S.; Zhang, Q.; Tian, X.; Fan, S.; Huang, J.; Whiting, A. Highly Selective Halogenation of Unactivated C(Sp 3)-H with NaX under Co-Catalysis of Visible Light and Ag@AgX. *Green Chem.* **2018**, *20* (20), 4729–4737.

(4) Düsel, S. J. S.; König, B. Oxidative Photochlorination of Electron-Rich Arenes via in Situ Bromination. *European J. Org. Chem.* **2019**, 1–6.

(5) Bonciolini, S.; Noël, T.; Capaldo, L. Synthetic Applications of Photocatalyzed Halogen-Radical Mediated Hydrogen Atom Transfer for C−H Bond Functionalization. *European J. Org. Chem.* **2022**, *2022* (34).

(6) Lin, R.; Amrute, A. P.; Pérez-Ramírez, J. Halogen-Mediated Conversion of Hydrocarbons to Commodities. *Chem. Rev.* **2017**, *117* (5), 4182–4247.

(7) Rohe, S.; Morris, A. O.; McCallum, T.; Barriault, L. Hydrogen Atom Transfer Reactions via Photoredox Catalyzed Chlorine Atom Generation. *Angew. Chemie Int. Ed.* **2018**, *57* (48), 15664–15669.

(8) Xu, P.; Chen, P. Y.; Xu, H. C. Scalable Photoelectrochemical Dehydrogenative Cross-Coupling of Heteroarenes with Aliphatic C−H Bonds. *Angew. Chemie - Int. Ed.* **2020**, *59* (34), 14275–14280.

(9) Deng, H. P.; Zhou, Q.; Wu, J. Microtubing-Reactor-Assisted Aliphatic C−H Functionalization with HCl as a Hydrogen-Atom-Transfer Catalyst Precursor in Conjunction with an Organic Photoredox Catalyst. *Angew. Chemie - Int. Ed.* **2018**, *57* (39), 12661–12665.

(10) Yang, Q.; Wang, Y. H.; Qiao, Y.; Gau, M.; Carroll, P. J.; Walsh, P. J.; Schelter, E. J. Photocatalytic C-H Activation and the Subtle Role of Chlorine Radical Complexation in Reactivity. *Science* **2021**, *372* (6544), 847–852.
(11) Panetti, G. B.; Yang, Q.; Gau, M. R.; Carroll, P. J.; Walsh, P. J.; Schelter, E. J. Discovery and Mechanistic Investigation of Photoinduced Sp3 C–H Activation of Hydrocarbons by the Simple Anion Hexachlorotitanate. *Chem Catal.* **2022**, *2* (4), 853–866.
(12) Ohkubo, K.; Fujimoto, A.; Fukuzumi, S. Metal-Free Oxygenation of Cyclohexane with Oxygen Catalyzed by 9-Mesityl-10-Methylacridinium and Hydrogen Chloride under Visible Light Irradiation. *Chem. Commun.* **2011**, *47* (30), 8515–8517.
(13) Hirscher, N. A.; Ohri, N.; Yang, Q.; Zhou, J.; Anna, J. M.; Schelter, E. J.; Goldberg, K. I. A Metal-Free, Photocatalytic Method for Aerobic Alkane Iodination. *J. Am. Chem. Soc.* **2021**, *143* (46), 19262–19267.
(14) Gygi, D.; Gonzalez, M. I.; Hwang, S. J.; Xia, K. T.; Qin, Y.; Johnson, E. J.; Gygi, F.; Chen, Y. S.; Nocera, D. G. Capturing the Complete Reaction Profile of a C-H Bond Activation. *J. Am. Chem. Soc.* **2021**, *143* (16), 6060–6064.
(15) Gonzalez, M. I.; Gygi, D.; Qin, Y.; Zhu, Q.; Johnson, E. J.; Chen, Y. S.; Nocera, D. G. Taming the Chlorine Radical: Enforcing Steric Control over Chlorine-Radical-Mediated C-H Activation. *J. Am. Chem. Soc.* **2022**, *144* (3), 1464–1472.
(16) Shields, B. J.; Doyle, A. G. Direct C(Sp3)-H Cross Coupling Enabled by Catalytic Generation of Chlorine Radicals. *J. Am. Chem. Soc.* **2016**, *138* (39), 12719–12722.
(17) Wang, Y. H.; Yang, Q.; Walsh, P. J.; Schelter, E. J. Light-Mediated Aerobic Oxidation of C(Sp3)-H Bonds by a Ce(Iv) Hexachloride Complex. *Org. Chem. Front.* **2022**, 2612–2620.
(18) Li, Z.; Luo, L.; Li, M.; Chen, W.; Liu, Y.; Yang, J.; Xu, S. M.; Zhou, H.; Ma, L.; Xu, M.; Kong, X.; Duan, H. Photoelectrocatalytic C–H Halogenation over an Oxygen Vacancy-Rich TiO2 Photoanode. *Nat. Commun.* **2021**, *12* (1), 1–13.
(19) Li, P.; Deetz, A. M.; Hu, J.; Meyer, G. J.; Hu, K. Chloride Oxidation by One- or Two-Photon Excitation of N -Phenylphenothiazine. *J. Am. Chem. Soc.* **2022**, *144* (38), 17604–17610.
(20) Kim, J. Y.; Lee, J.-W.; Jung, H. S.; Shin, H.; Park, N.-G. High-Efficiency Perovskite Solar Cells. *Chem. Rev.* **2020**, *120* (15), 7867–7918.
(21) Jošt, M.; Kegelmann, L.; Korte, L.; Albrecht, S. Monolithic Perovskite Tandem Solar Cells: A Review of the Present Status and Advanced Characterization Methods Toward 30% Efficiency. *Adv. Energy Mater.* **2020**, *10* (26), 1904102.
(22) Peter, L. "Sticky Electrons" Transport and Interfacial Transfer of Electrons in the Dye-Sensitized Solar Cell. *Acc. Chem. Res.* **2009**, *42* (11), 1839–1847.
(23) Gong, J.; Sumathy, K.; Qiao, Q.; Zhou, Z. Review on Dye-Sensitized Solar Cells (DSSCs): Advanced Techniques and Research Trends. *Renew. Sustain. Energy Rev.* **2017**, *68*, 234–246.
(24) Hagfeldt, A.; Boschloo, G.; Sun, L.; Kloo, L.; Pettersson, H. Dye-Sensitized Solar Cells. *Chem. Rev.* **2010**, *110* (11), 6595–6663.
(25) McDaniel, N. D.; Bernhard, S. Solar Fuels: Thermodynamics, Candidates, Tactics, and Figures of Merit. *Dalt. Trans.* **2010**, *39* (42), 10021–10030.
(26) Powers, D. C.; Hwang, S. J.; Zheng, S. L.; Nocera, D. G. Halide-Bridged Binuclear HX-Splitting Catalysts. *Inorg. Chem.* **2014**, *53* (17), 9122–9128.
(27) Heyduk, A. F.; Nocera, D. G. Hydrogen Produced from Hydrohalic Acid Solutions by a Two-Electron Mixed-Valence Photocatalyst. *Science* **2001**, *293* (5535), 1639–1641.

(28) Hwang, S. J.; Powers, D. C.; Maher, A. G.; Anderson, B. L.; Hadt, R. G.; Zheng, S.-L.; Chen, Y.-S.; Nocera, D. G. Trap-Free Halogen Photoelimination from Mononuclear Ni(III) Complexes. *J. Am. Chem. Soc.* **2015**, *137* (20), 6472–6475.
(29) Powers, D. C.; Anderson, B. L.; Nocera, D. G. Two-Electron HCl to H2 Photocycle Promoted by Ni(II) Polypyridyl Halide Complexes. *J. Am. Chem. Soc.* **2013**, *135* (50), 18876–18883.
(30) Du, J.; Chen, Z.; Chen, C.; Meyer, T. J. A Half-Reaction Alternative to Water Oxidation: Chloride Oxidation to Chlorine Catalyzed by Silver Ion. *J. Am. Chem. Soc.* **2015**, *137* (9), 3193–3196.
(31) Troian-Gautier, L.; Swords, W. B.; Meyer, G. J. Iodide Photoredox and Bond Formation Chemistry. *Acc. Chem. Res.* **2019**, *52* (1), 170–179.
(32) Swords, W. B.; Li, G.; Meyer, G. J. Iodide Ion Pairing with Highly Charged Ruthenium Polypyridyl Cations in CH3CN. *Inorg. Chem.* **2015**, *54* (9), 4512–4519.
(33) Lakowicz, J. R. *Principles of Fluorescence Spectroscopy*, 3rd ed.; Springer US: New York, 2006.
(34) Troian-Gautier, L.; Beauvilliers, E. E.; Swords, W. B.; Meyer, G. J. Redox Active Ion-Paired Excited States Undergo Dynamic Electron Transfer. *J. Am. Chem. Soc.* **2016**, *138* (51), 16815–16826.
(35) Deetz, A. M.; Meyer, G. J. Resolving Halide Ion Stabilization through Kinetically Competitive Electron Transfers. *JACS Au* **2022**, *2*, 985–995.
(36) Nocera, D. G. Chemistry of Personalized Solar Energy. *Inorg. Chem.* **2009**, *48* (21), 10001–10017.
(37) Li, J.-H.; Wang, J.-T.; Mao, Z.-W.; Ji, L.-N. Synthesis, Interaction with DNA and Nuclease Activity of Zinc Complexes of 2,2′-Bipyridine Derivatives with Tetraalkylammonium Groups. *J. Coord. Chem.* **2009**, *62* (3), 446–455.
(38) Fulmer, G. R.; Miller, A. J. M.; Sherden, N. H.; Gottlieb, H. E.; Nudelman, A.; Stoltz, B. M.; Bercaw, J. E.; Goldberg, K. I. NMR Chemical Shifts of Trace Impurities: Common Laboratory Solvents, Organics, and Gases in Deuterated Solvents Relevant to the Organometallic Chemist. *Organometallics* **2010**, *29* (9), 2176–2179.
(39) Thordarson, P. Supramolecular.org.
(40) Brynn Hibbert, D.; Thordarson, P. The Death of the Job Plot, Transparency, Open Science and Online Tools, Uncertainty Estimation Methods and Other Developments in Supramolecular Chemistry Data Analysis. *Chem. Commun.* **2016**, *52* (87), 12792–12805.
(41) Thordarson, P. Determining Association Constants from Titration Experiments in Supramolecular Chemistry. *Chem. Soc. Rev.* **2011**, *40* (3), 1305–1323.
(42) Deaton, J. C.; Castellano, F. N. Archetypal Iridium(III) Compounds for Optoelectronic and Photonic Applications. In *Iridium(III) in Optoelectronic and Photonics Applications*; 2017; pp 1–69.
(43) Deetz, A. M.; Troian-Gautier, L.; Wehlin, S. A. M.; Piechota, E. J.; Meyer, G. J. On the Determination of Halogen Atom Reduction Potentials with Photoredox Catalysts. *J. Phys. Chem. A* **2021**, *125* (42), 9355–9367.
(44) Zysman-Colman, E.; Slinker, J. D.; Parker, J. B.; Malliaras, G. G.; Bernhard, S. Improved Turn-On Times of Light-Emitting Electrochemical Cells. *Chem. Mater.* **2008**, *20* (2), 388–396.
(45) Saund, S. S.; Siegler, M. A.; Thoi, V. S. Electrochemical Degradation of a Dicationic Rhenium Complex via Hoffman-Type Elimination. *Inorg. Chem.* **2021**, *60* (17), 13011–

13020.
(46) Kerzig, C.; Guo, X.; Wenger, O. S. Unexpected Hydrated Electron Source for Preparative Visible-Light Driven Photoredox Catalysis. *J. Am. Chem. Soc.* **2019**, *141* (5), 2122–2127.
(47) Thordarson, P. Supramolecular.Org.
(48) Turlington, M. D.; Deetz, A. M.; Vitt, D.; Meyer, G. J. Photocatalyst Assemblies with Two Halide Ions. *J. Photochem. Photobiol.* **2022**, *9*, 100090.
(49) Troian-Gautier, L.; Wehlin, S. A. M.; Meyer, G. J. Photophysical Properties of Tetracationic Ruthenium Complexes and Their Ter-Ionic Assemblies with Chloride. *Inorg. Chem.* **2018**, *57* (19), 12232–12244.
(50) Wehlin, S. A. M.; Troian-Gautier, L.; Sampaio, R. N.; Marcélis, L.; Meyer, G. J. Ter-Ionic Complex That Forms a Bond Upon Visible Light Absorption. *J. Am. Chem. Soc.* **2018**, *140* (25), 7799–7802.
(51) Adriaenssens, L.; Gil-Ramírez, G.; Frontera, A.; Quiñonero, D.; Escudero-Adán, E. C.; Ballester, P. Thermodynamic Characterization of Halide−π Interactions in Solution Using "Two-Wall" Aryl Extended Calix[4]Pyrroles as Model System. *J. Am. Chem. Soc.* **2014**, *136* (8), 3208–3218.
(52) Teets, T. S.; Nocera, D. G. Photocatalytic Hydrogen Production. *Chem. Commun.* **2011**, *47* (33), 9268–9274.
(53) Wehlin, S. A. M. M.; Troian-Gautier, L.; Li, G.; Meyer, G. J. Chloride Oxidation by Ruthenium Excited-States in Solution. *J. Am. Chem. Soc.* **2017**, *139* (37), 12903–12906.
(54) Cook, T. R.; Surendranath, Y.; Nocera, D. G. Chlorine Photoelimination from a Diplatinum Core: Circumventing the Back Reaction. *J. Am. Chem. Soc.* **2009**, *131* (1), 28–29.

TOC Graphic

Synopsis: The photoluminescent excited state of four Ir photocatalysts bearing two quaternary amine groups were quenched by chloride ions through two competitive mechanisms: 1) a ‘static’ mechanism; and 2) a dynamic mechanism. Chloride-ion pairing interactions quantified by ^{1}H NMR revealed photocatalyst dependent structures and association constants. Association of chloride with these photocatalysts in the ground state enables intra-ionic chloride oxidation on a rapid, nanosecond timescale.